Arylselanyl-motifs in hierarchically-structured mesoporous phenolic polymers: Efficient adsorption sites for the Hg^{2+} ions

Vishnu Selladurai and Selvakumar Karuthapandi*

Department of Chemistry, School of Advanced Sciences, VIT-AP University, India

Corresponding author email-id. selvakumar.k@vitap.ac.in

Electronic Supplementary Information (ESI)

Table of Contents

1. Synthesis of Rh-B-imine

Rhodamine-B hydrazide (**1**) and Rhodamine-B imine (Rh-B-imine) were synthesized based on literature reports.[1-3] **Figure S1** describes the synthesis of Rh-B imine. In a double-necked round-bottomed flask, 0.208 g (0.45mmol) of rhodamine-B hydrazide and 0.043 mL (0.45 mmol) of 2-pyridine carboxaldehyde were placed. Methanol and a few drops of acetic acid were added to the mixture and the content was refluxed for 2 hours. The resulting white precipitate (0.173 g, 74.3%) was filtered through a Buckner funnel using vacuum filtration, and the solid was then washed with methanol and dried under vacuum. HRMS $(ESI)^+$ *m/z* $[M + H]^+$ calcd for $C_{34}H_{35}N_5O_2$: 546.2864; found 546.2870. ^1H NMR (400 MHz, $CDCl_3$) δ 8.50 – 8.43 (m, 1H), 8.38 (s, 1H), 8.05 – 7.97 (m, 2H), 7.60 (td, *J* = 7.7, 1.7 Hz, 1H), 7.53 – 7.40 (m, 2H), 7.17 – 7.08 (m, 2H), 6.55 (d, *J* = 8.8 Hz, 2H), 6.45 (d, *J* = 2.6 Hz, 2H), 6.24 (dd, *J* = 8.8, 2.6 Hz, 2H), 3.31 (q, *J* = 7.1 Hz, 8H), 1.15 (t, *J* = 7.0 Hz, 12H). FTIR (KBr): 3444, 2974, 2877, 1729, 1617, 1520, 1364, 1304, 1222, 1118, 969, 782, 521 cm^{-1}.

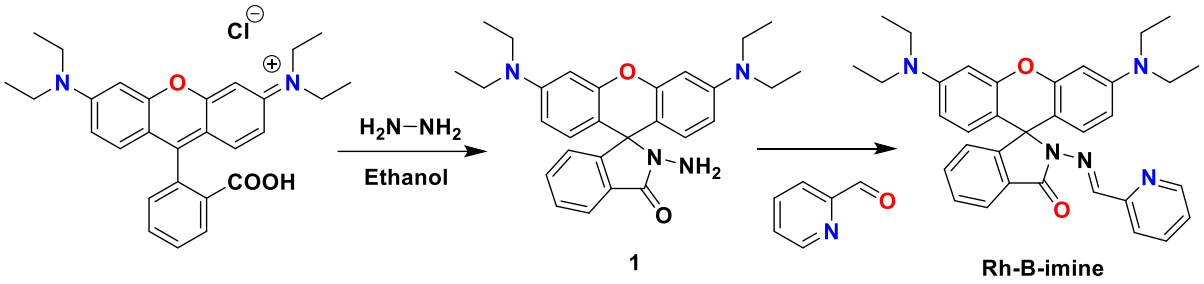

Figure S1. Synthesis of Rhodamine – B imine (Rh-B-imine) probe.

2. Mechanism for selenation and polymerization

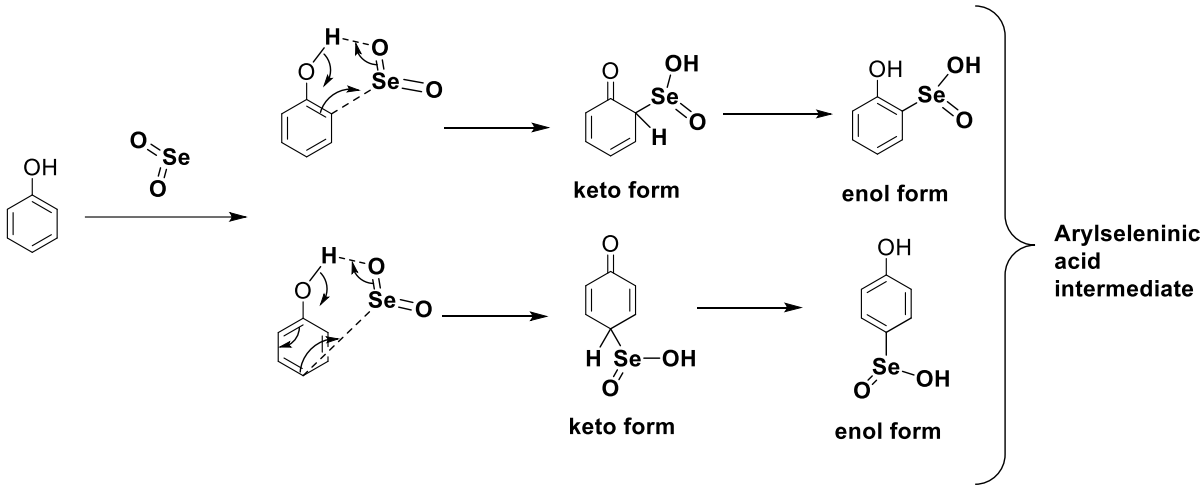

Figure S2: Reaction mechanism for the formation of arylseleninic acid intermediate.

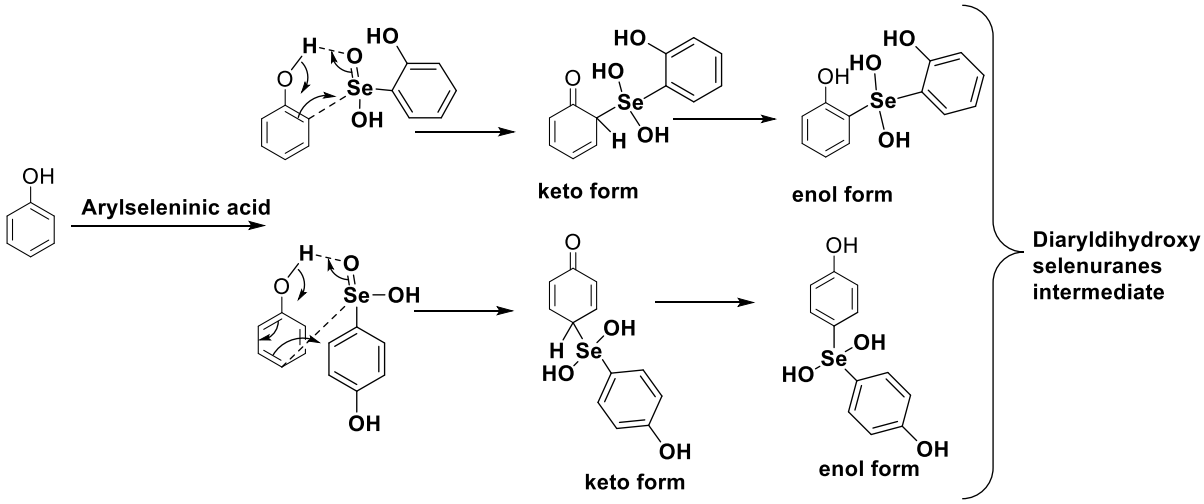

Figure S3: Reaction mechanism for the formation of diaryl dihydroxyselenuranes intermediate.

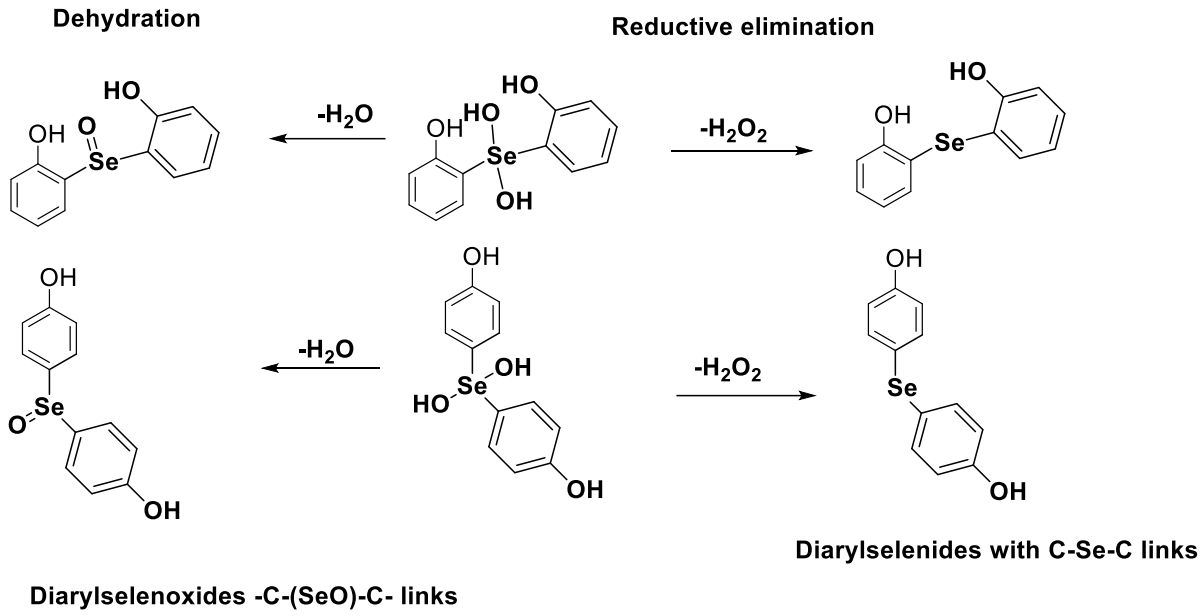

Figure S4: Reaction mechanism for the formation of diarylselenide monomers.

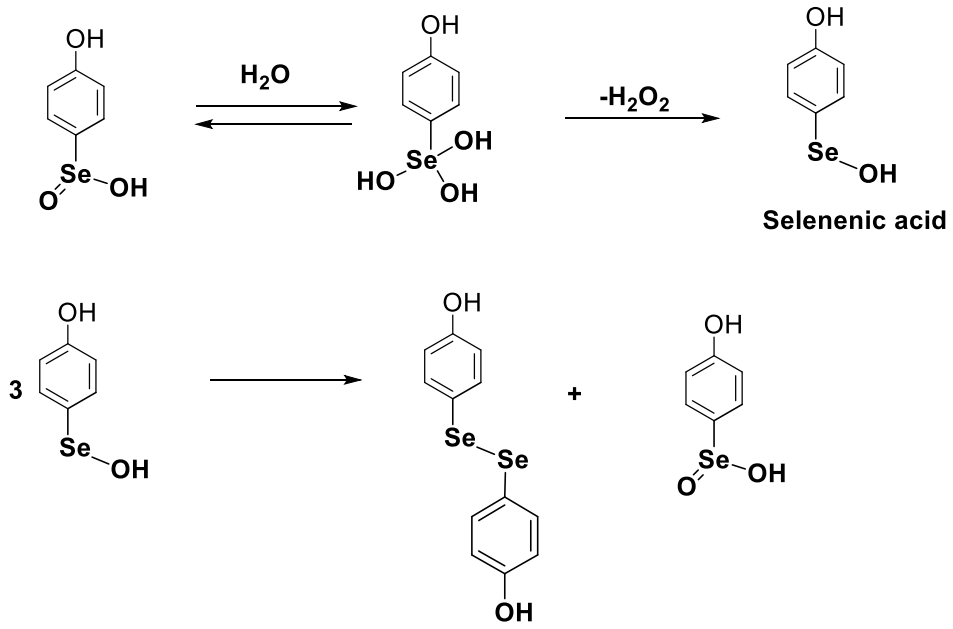

Figure S5: Reaction mechanism for the formation of diaryl-diselenide monomer.

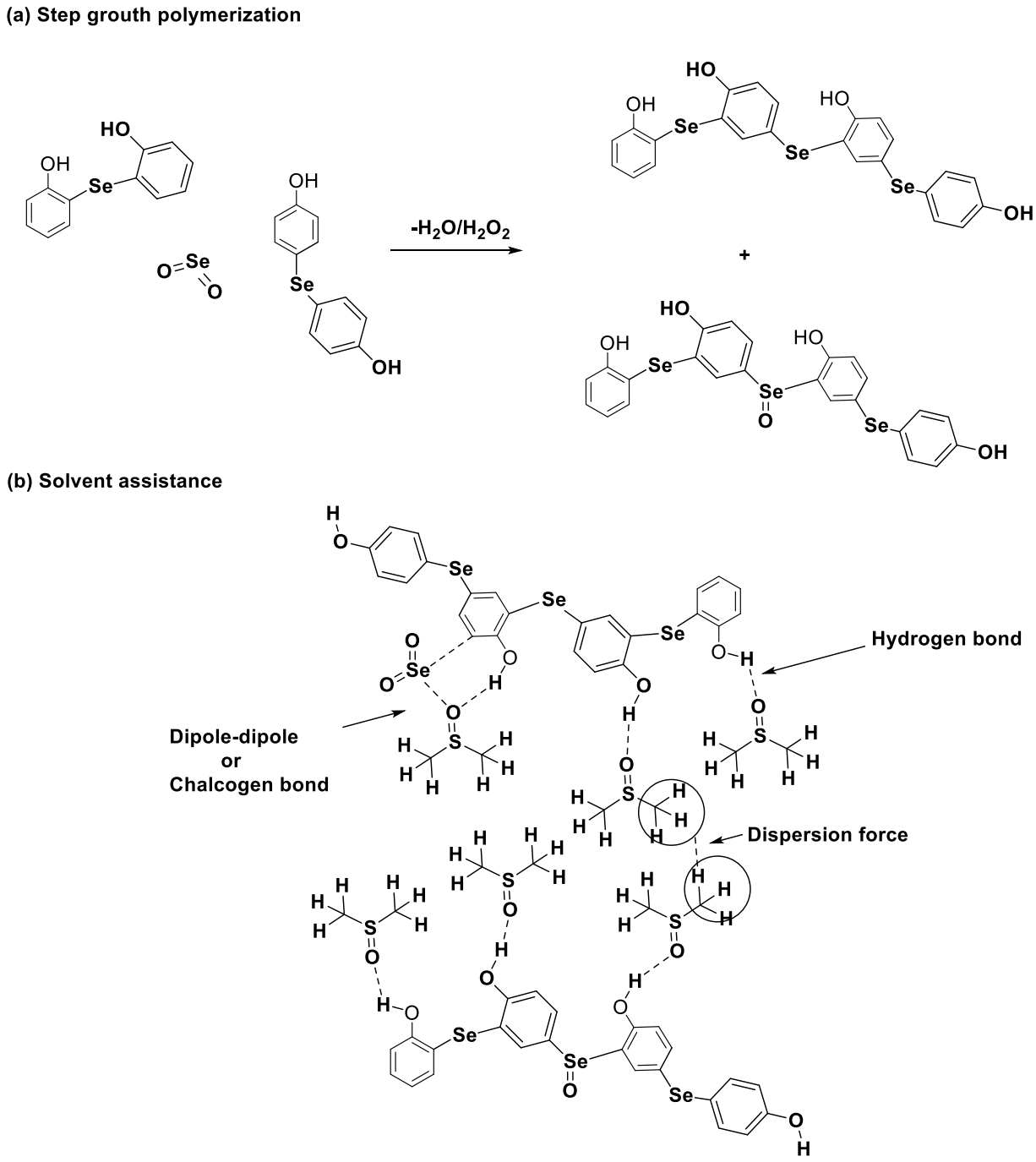

Figure S6: Mechanism for the (a) step growth polymerization (b) solvent assistance for polymerization

3. Spectrometric characterization of Rh-B-imine

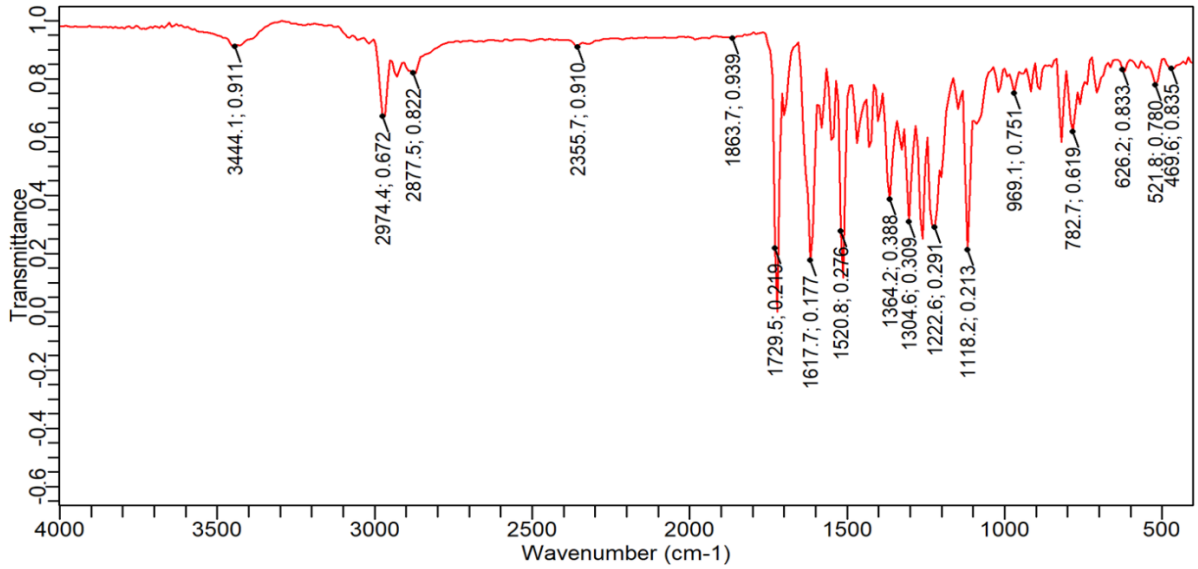

Figure S7. FTIR – spectrum for Rh-B-imine

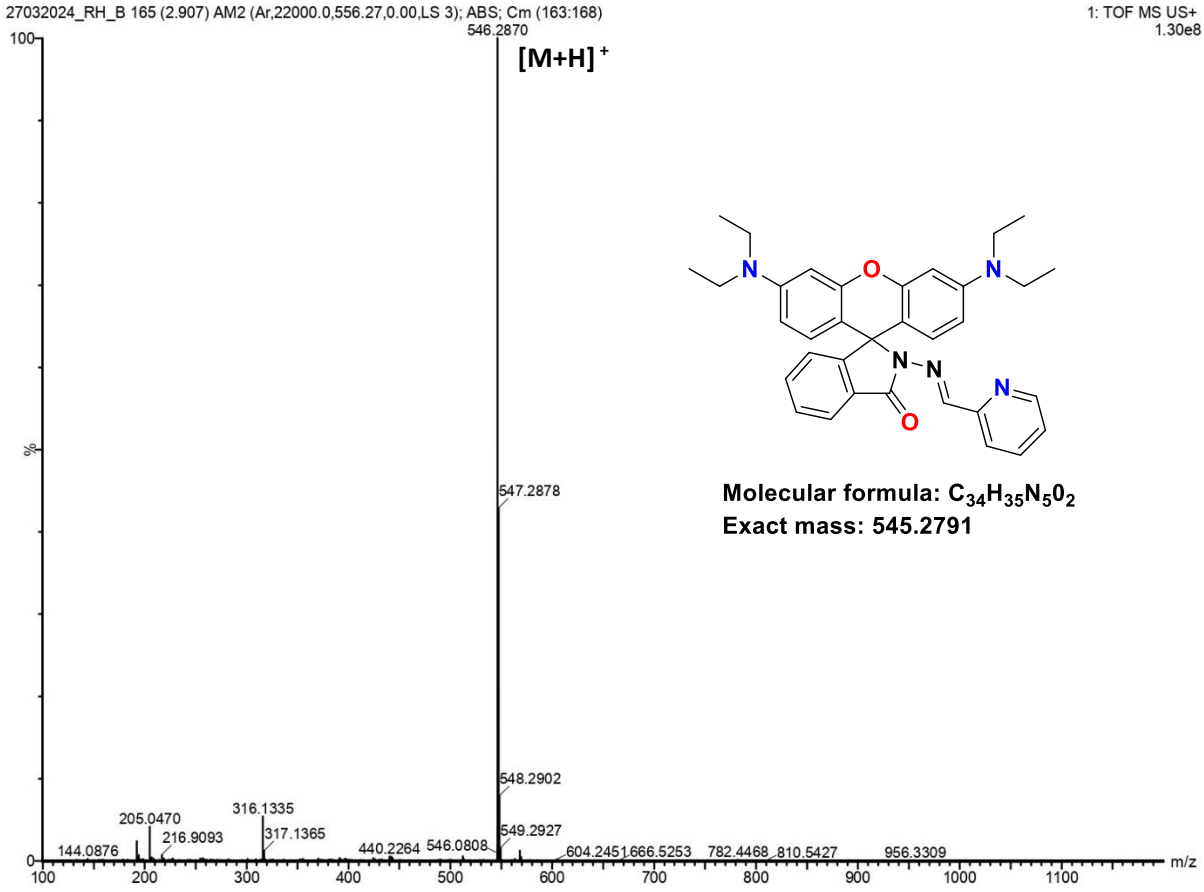

Figure S8. HRMS $(ESI)^+$ – spectrum for Rh-B-imine

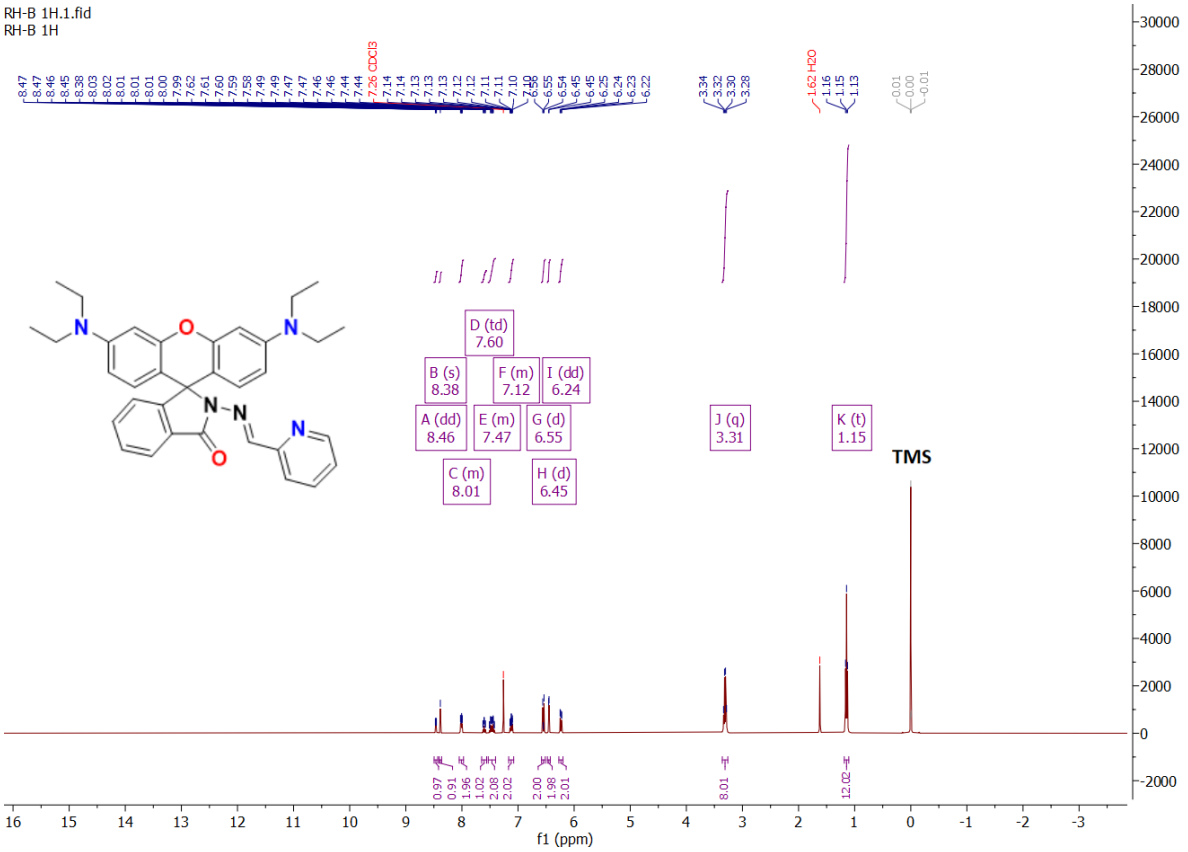

Figure S9. ^{1}H – NMR spectral studies for Rh-B-imine

4. Elemental mapping and EDAX analysis of Se-PR 1 and Se-PR 2

(a)

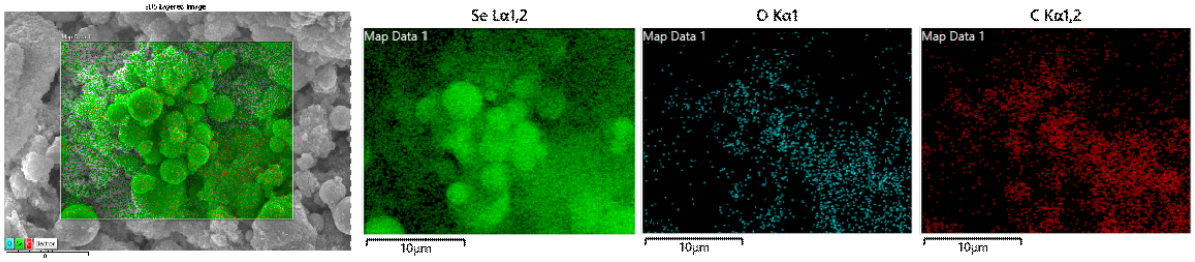

(b)

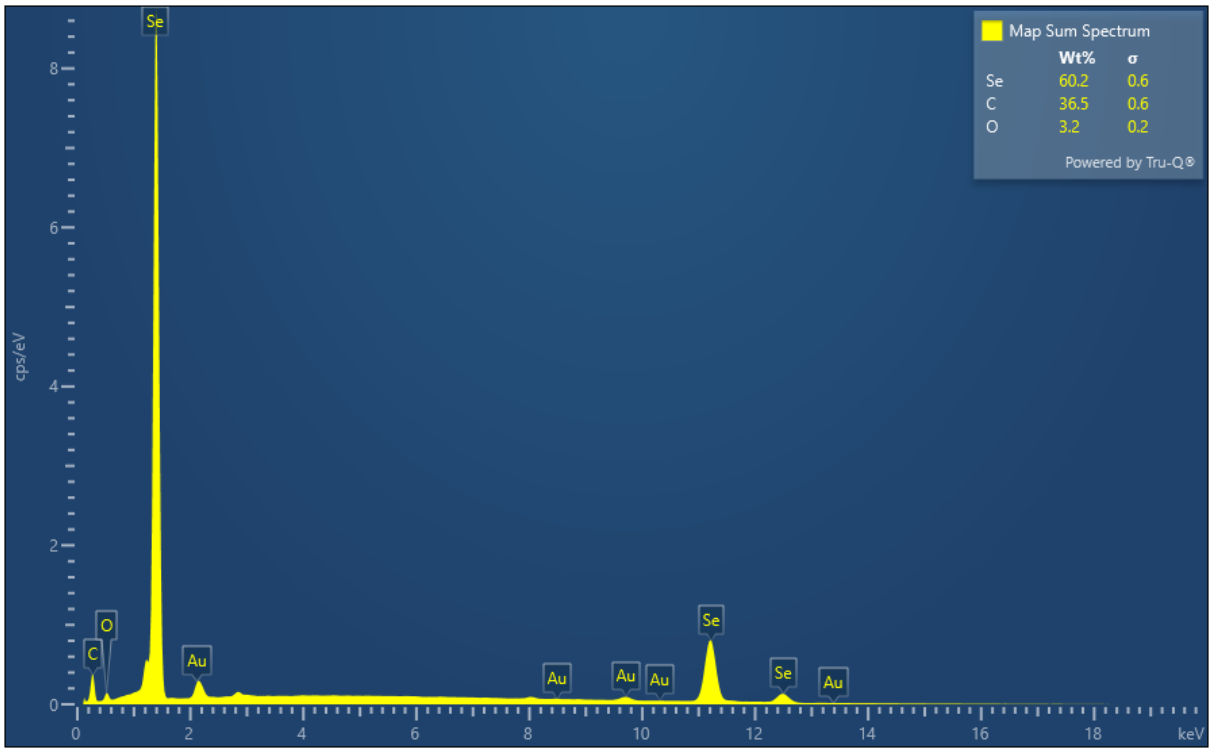

Figure S10. (a) Elemental mapping and (b) EDAX – Spectral Analysis of pristine Se-PR **1**

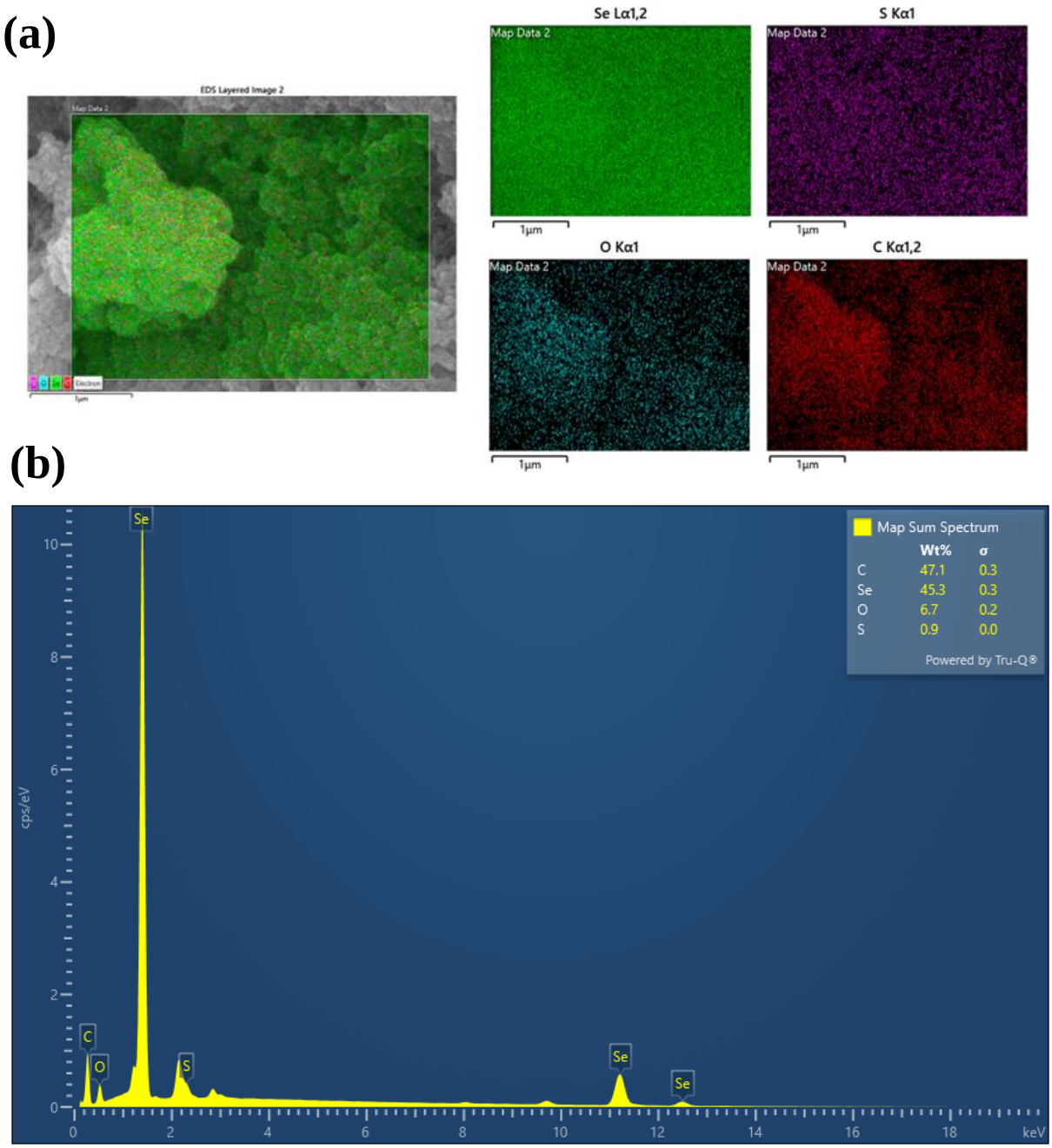

Figure S11. (a) Elemental mapping and (b) EDAX – Spectral Analysis of pristine Se-PR **2**

5. Freundlich adsorption isotherm (linear fit model) for the Hg^{2+} adsorption on Se-PR 1 and Se-PR 2

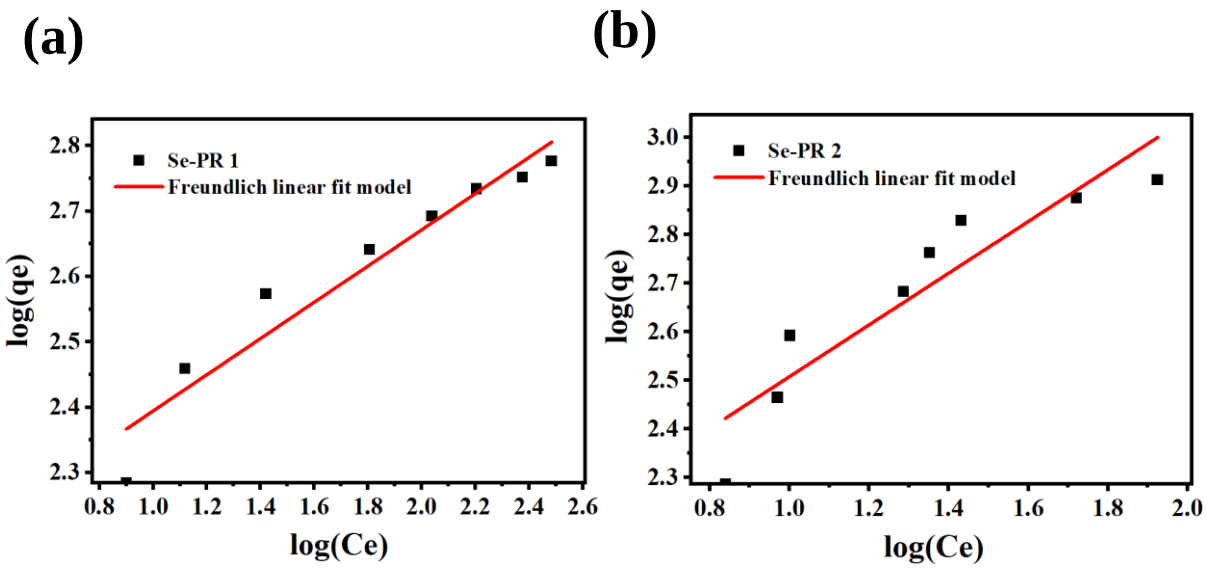

Figure S12: Freundlich linear fit model for the (a) Hg^{2+} adsorption on Se-PR **1** and (b) Hg^{2+} adsorption on Se-PR **2**.

Table S1: Freundlich adsorption isotherm model parameters for the adsorption of Hg^{2+} ions on Se-PR **1** and Se-PR **2**.

	Intercept	Slope	n	k_f (mg/g) ((L/mg)$^{1/n}$)	R^2
Se-PR **1**	2.11716	0.2772	3.61	1.31×10^2	0.9199
Se-PR **2**	1.97499	0.5327	1.88	9.4×10^1	0.8318

6. Comparison FT-IR spectrum pristine and Hg^{2+} containing Se-PR 1

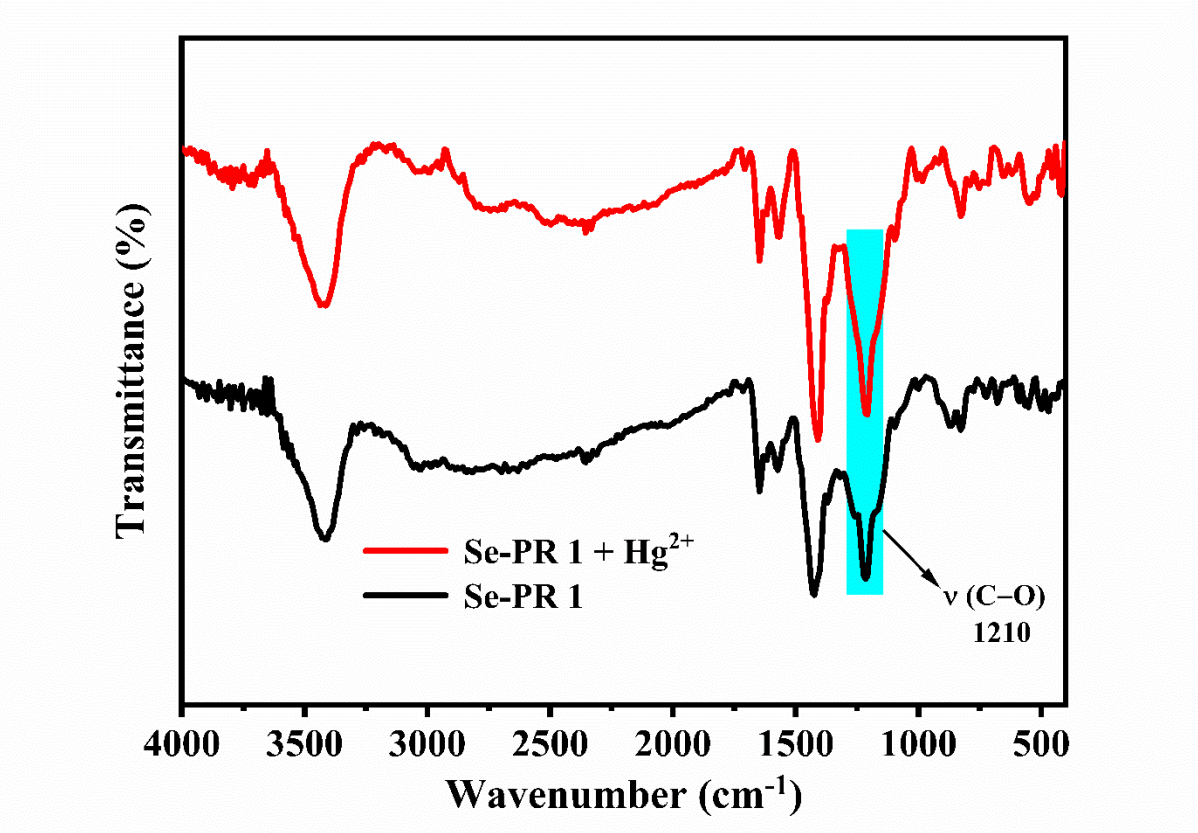

Figure S13: Overlay of FT-IR spectrum of pristine and Hg^{2+} treated Se-PR **1**

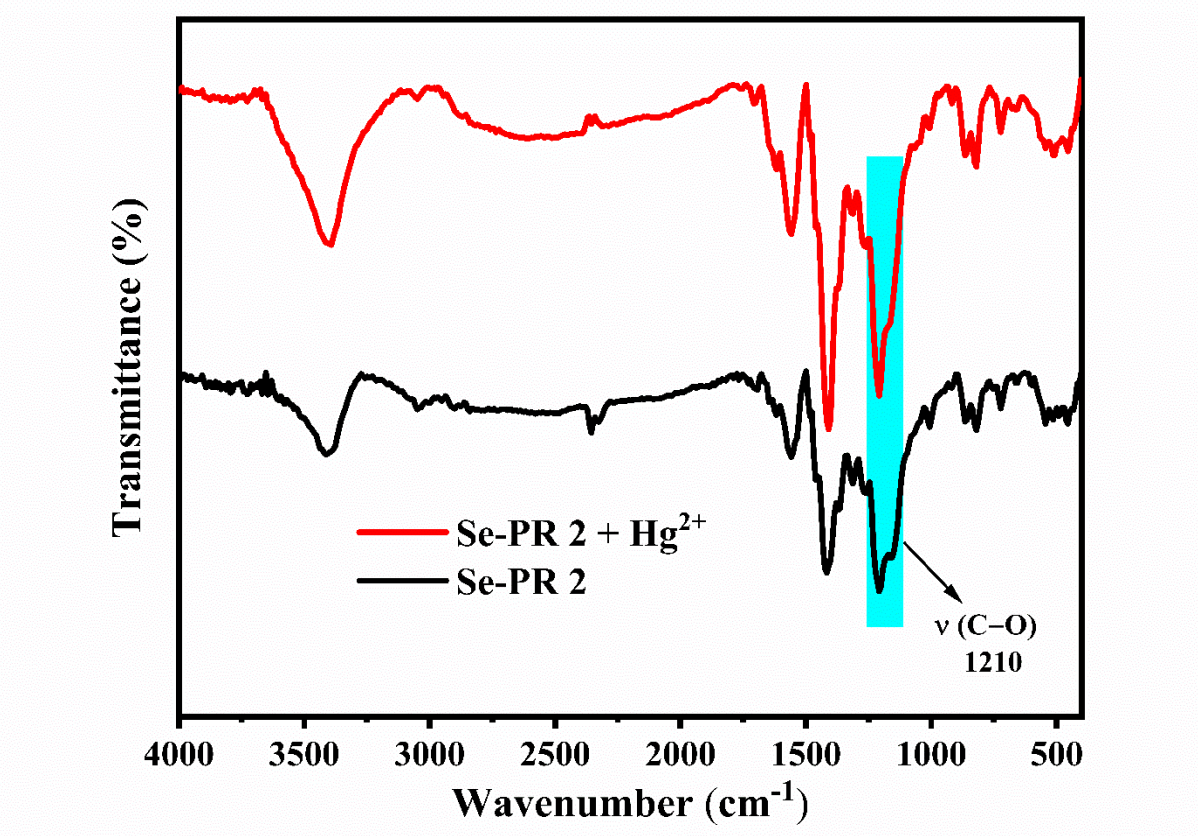

Figure S14: Overlay of FT-IR spectrum of pristine and Hg^{2+} treated Se-PR **2**

7. Comparison of FE-SEM images of pristine Se-PR 1 and Se-PR 2 with their respective Hg^{2+} treated material

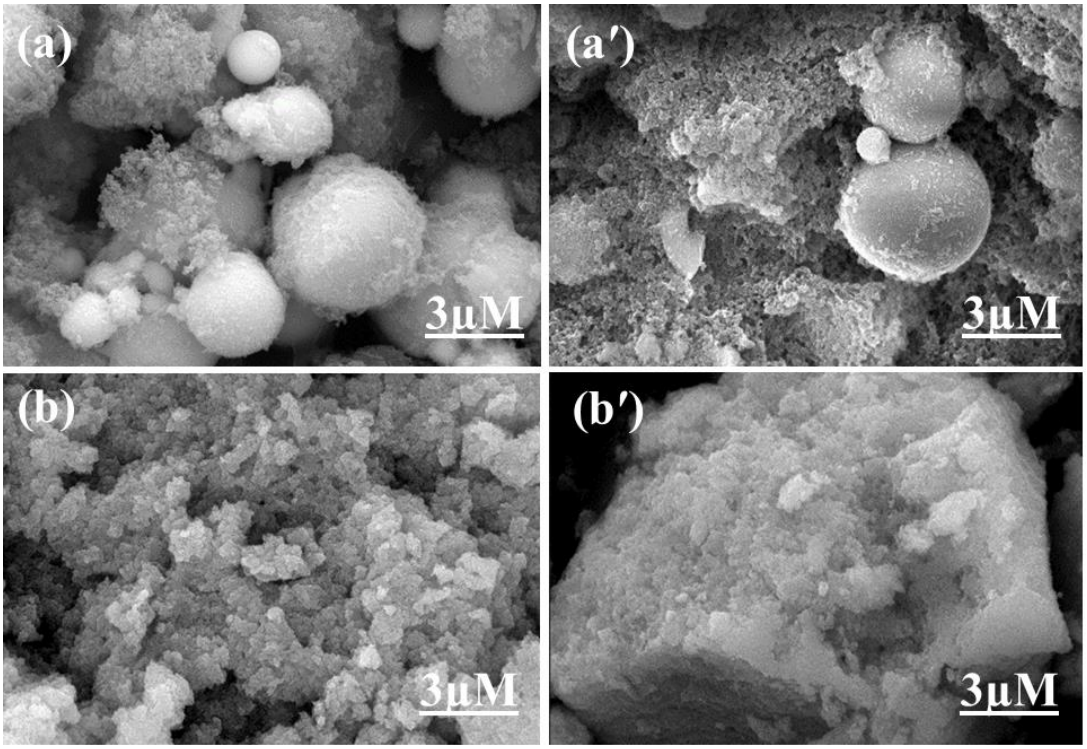

Figure S15: (a) Pristine Se-PR **1** and (a′) Hg^{2+} treated Se-PR **1**; (b) Pristine Se-PR **2** and (b′) Hg^{2+} treated Se-PR **2**

8. Elemental mapping and EDAX analysis of Hg^{2+} treated Se-PR 1 and Se-PR 2

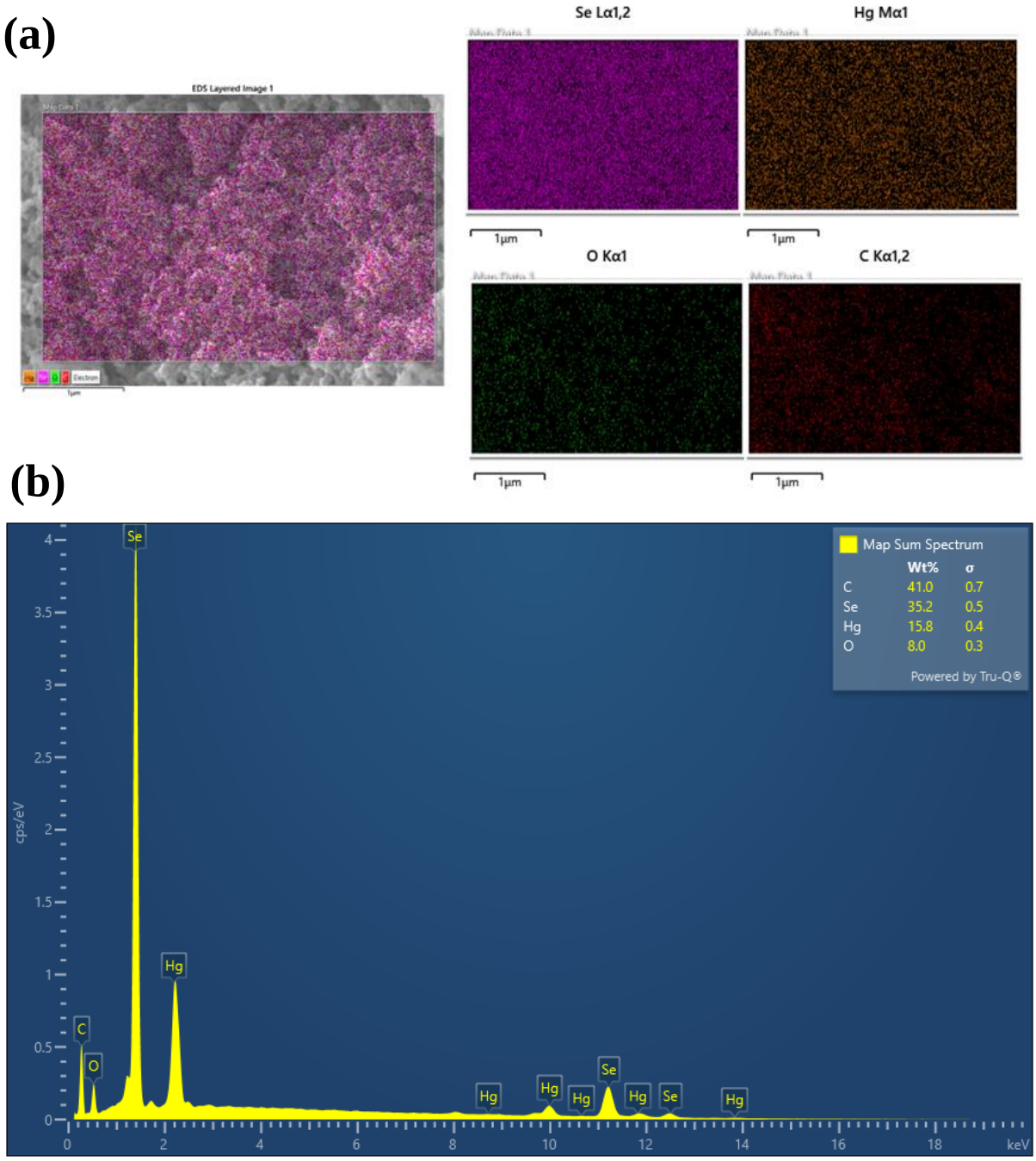

Figure S16: (a) Elemental mapping and (b) EDAX – Spectral Analysis of Se-PR **1** with adsorbed Hg^{2+} ions

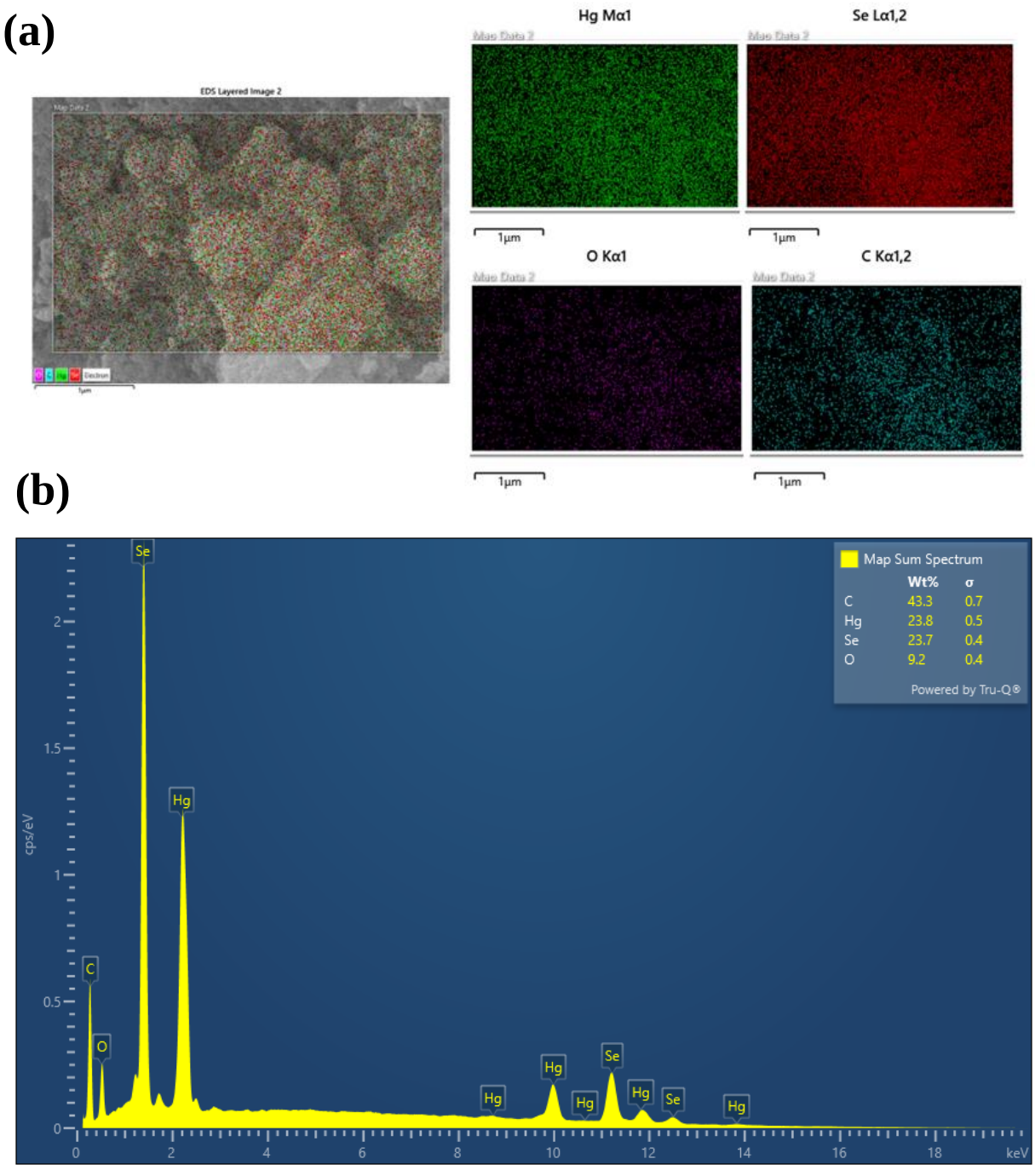

Figure S17: (a) Elemental mapping and (b) EDAX – Spectral Analysis of Se-PR **2** with adsorbed Hg^{2+} ions

9. Comparative Study of powder XRD analysis of Se-PR 2 and recycled Se-PR 2

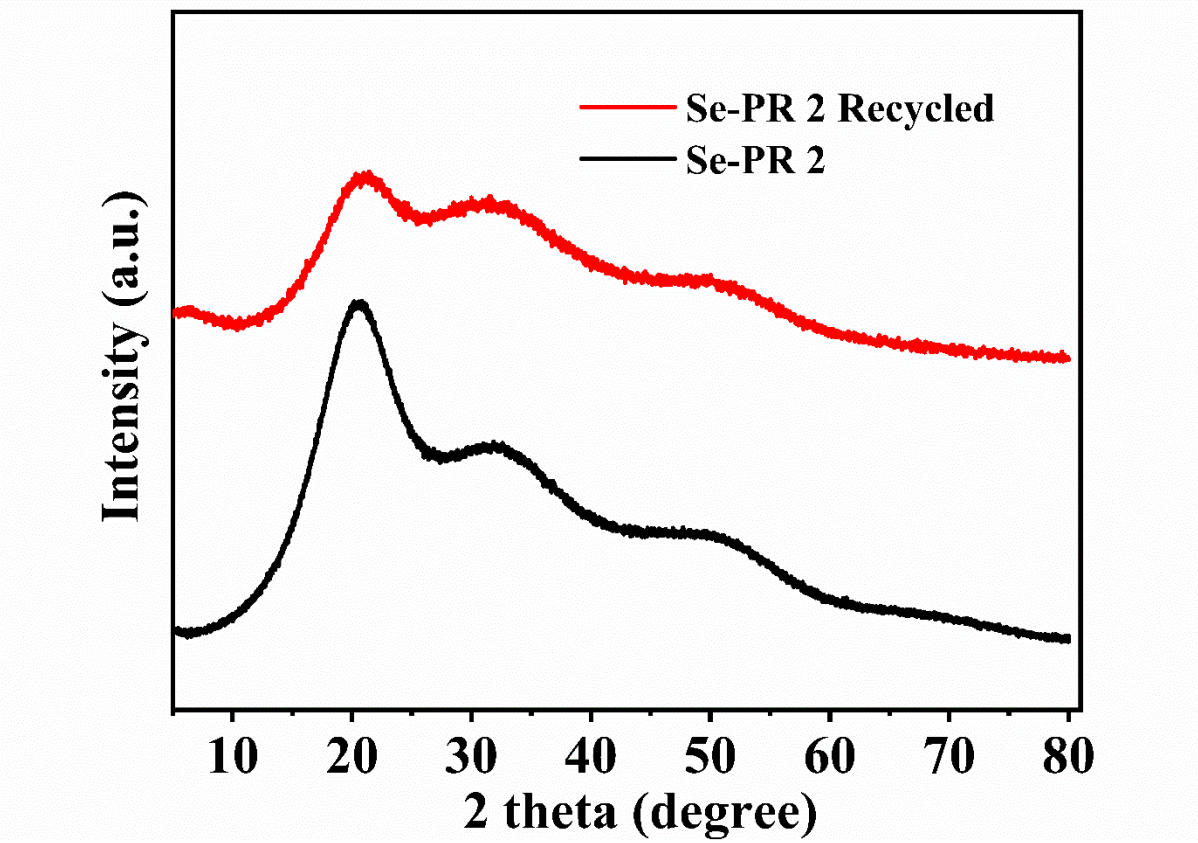

Figure S18: Powder XRD of (a) Pristine polymer of Se-PR 2 and (b) Recycled Se-PR 2.

10. Comparative Study of FE-SEM Images of Se-PR 2 and recycled Se-PR 2

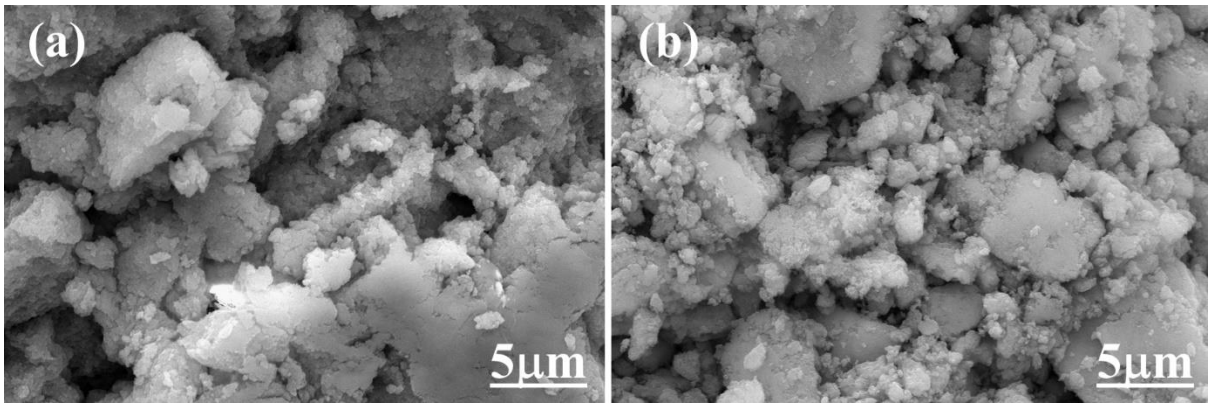

Figure S19: FE-SEM images of (a) Pristine polymer of Se-PR 2 and (b) Recycled Se-PR 2.

11. Comparative Study of nitrogen sorption and desorption analysis of Pristine Se-PR 2 and recycled Se-PR 2

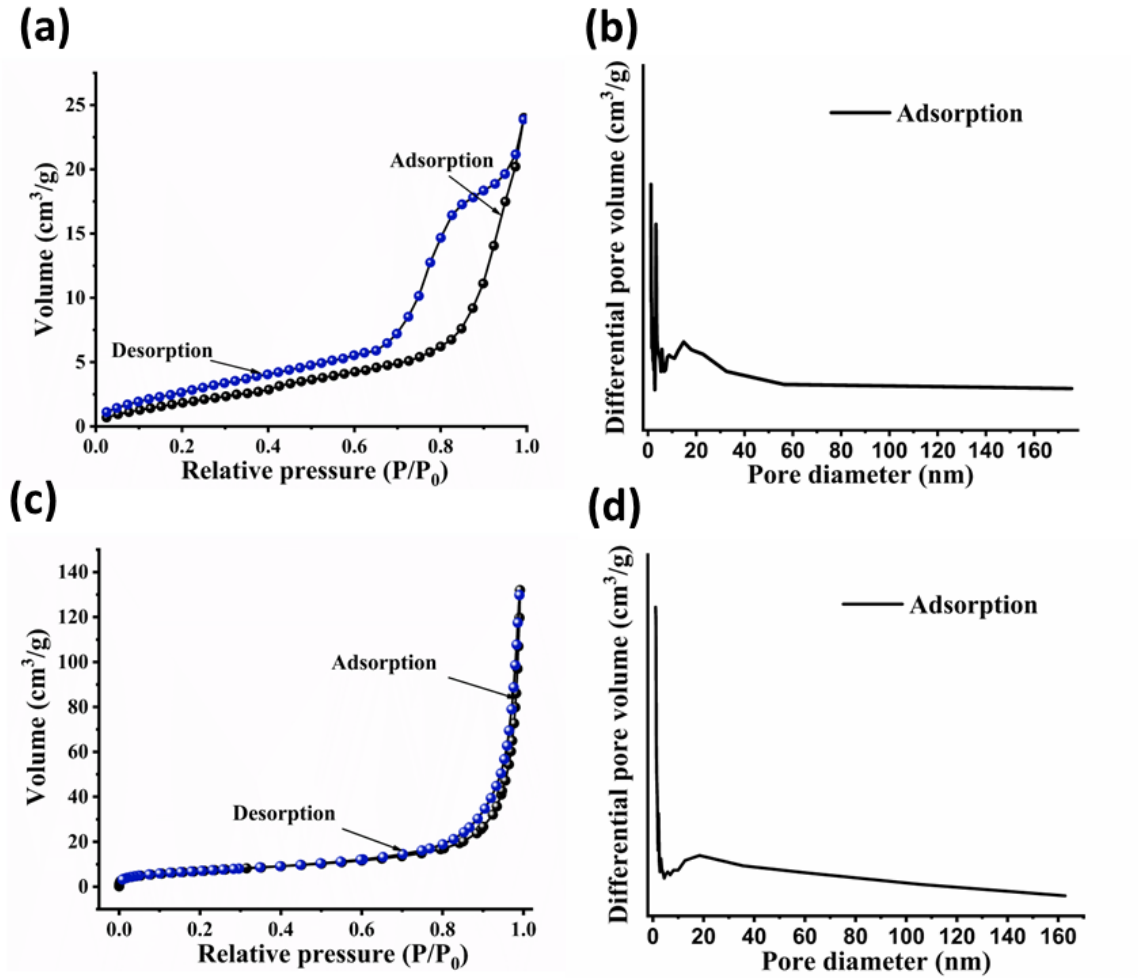

Figure S20: (a) and (b) N_2 sorption isotherm and BJH pore size distribution curve of pristine Se-PR **2**, (c) and (d) N_2 sorption isotherm and BJH pore size distribution curve of recycled Se-PR **2**.

Table S2: Surface area, pore volume and average pore size

Polymer	**BET surface area (m^2g^{-1})**	**Total Pore volume (cc g^{-1})**	**Average Pore size (nm)**
Pristine Se-PR **2**	16.568	0.041	1.226
Recycled Se-PR **2**	38.862	0.184	1.045

12. Comparative Study of EDAX analysis of Hg^{2+} loaded Se-PR 2 and recycled Se-PR 2

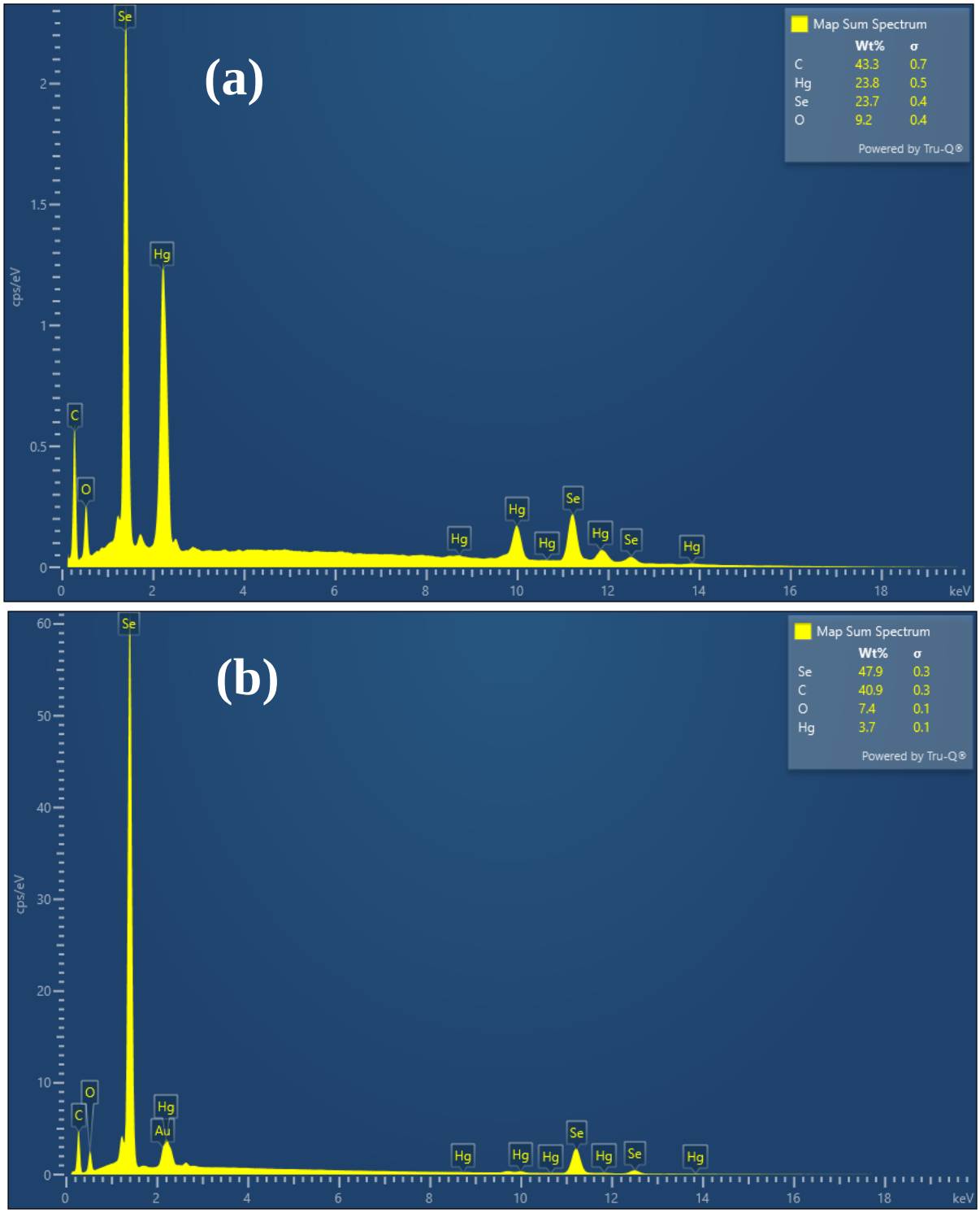

Figure S21: EDAX – Spectral Analysis of (a) Hg^{2+} loaded Se-PR **2** (b) recycled Se-PR **2**

13. References:

1. P. Mahato, S. Saha, P. Das, H. Agarwalla and A. Das, *RSC adv.* 2014, **4**, 36140-36174.
2. K. N. Kim, M. G. Choi, J. H. Noh, S. D. Ahn and S. K. Chang, *Bull Korean Chem Soc.*, 2008, **29**, 571-574.
3. A. Leite, A. M. Silva, L. Cunha-Silva, B. de Castro, P. Gameiro and M. Rangel, *Dalton Trans.*, 2013, **42**, 6110-6118.